Archives of Materials Science and Engineering

Volume 118
Issue 1
November 2022
Pages 5-28

International Scientific Journal
published monthly by the
World Academy of Materials
and Manufacturing Engineering

DOI: 10.5604/01.3001.0016.2442

An analysis of crystallographic texture and residual stresses of aluminium alloy RSA-501 after selected processes of twist extrusion (TE)

P. Byczkowska [a,*], J. Sawicki [a], B. Adamczyk-Cieślak [b], B. Januszewicz [a]

[a] Institute of Materials Science and Engineering, Faculty of Mechanical Engineering, Lodz University of Technology, Stefanowskiego Street 1/15, 90-924 Łódź, Poland

[b] Faculty of Materials Science and Engineering, Warsaw University of Technology, Wołoska Street 141, 02-507 Warsaw, Poland

* Corresponding e-mail address: paulina.byczkowska@p.lodz.pl

ORCID identifier: https://orcid.org/0000-0002-5429-7933 (P.B.)

ABSTRACT

Purpose: This study presents the residual stress analysis for the twist extrusion (TE) process after the experiment and numerical simulation and the analysis of the crystallographic texture changes and changes in hardness before and after the TE process for an RSA-501 aluminium alloy (Al; Mg5%; Mn1.5%; Sc0.8%; Zr0.4%).

Design/methodology/approach: Crystallographic textures were obtained with the PANAlytical Empyrean X-ray diffractometer. The stresses were measured by applying the X-ray method with the use of using the PROTO iXRD diffractometer.

Findings: The use of severe plastic deformation processes in the mass of the material leads to a significant change difference in the stress distribution in the workpiece and a change in texture compared to the reference material. The stress distribution in the sample cross-section and stress values varied and depended on the stage of the twisting process to which the surface was subjected. The highest stress (about 600 MPa) appears at the peaks of the front surface when exiting the twist area die TE. Higher stress values at the edges of the specimen are caused by friction (deformation) of the material against the die surface. The TE process strengthened – the highest crystallographic texture background level was 49%.

Practical implications: The conducted tests and the obtained results allow the determination of the process parameters and critical areas of the sample by carrying out a numerical simulation.

Originality/value: Microhardness increases due to the TE process and the largest values were observed at the edges. This phenomenon is confirmed by the numerical simulation results presented in this paper.

Keywords: Severe plastic deformation, Twist extrusion, Aluminium, FEM, Fine element method, Crystallographic texture, Stress, Hardness

Reference to this paper should be given in the following way:

P. Byczkowska, J. Sawicki, B. Adamczyk-Cieślak, B. Januszewicz, An analysis of crystallographic texture and residual stresses of aluminium alloy RSA-501 after selected processes of twist extrusion (TE), Archives of Materials Science and Engineering 118/1 (2022) 5-28. DOI: https://doi.org/10.5604/01.3001.0016.2442

PROPERTIES

1. Introduction

Severe Plastic Deformation (SPD) processing is a technique used in the production of materials – the purpose of which is to change stress distribution in the materials and form so-called 'deformation textures.' The texture is an important feature of polycrystalline materials, which may positively affect their properties. Textured materials demonstrate anisotropic behaviour. Anisotropy can be a desirable feature in some products, especially when their directional properties are important. In those cases, the material's texture can be used for specific applications. For example, the article [1] discusses the reinforcing mechanisms. The main enhancement mechanisms were grain refinement and texture modification. Other mechanisms within the sample interact depending on the phase of the process. This grain refinement was the dominant way to improve tensile strength during the first two deformation passes. On the other hand, the texture modification determined high ductility after three deformations. The authors noticed that thanks to using one of the SPD methods, CEE-AEC, it was possible to improve the grain structure and the microstructure's uniformity effectively.

This, naturally, requires the ability to shape it during technological processes such as SPD consciously. The most popular SPD (Fig. 1) techniques are HPT (High-Pressure Torsion) [2, 3-7], ECAP (Equal Channel Angular Pressing) [3,4, 8-11], TE (Twist Extrusion) [12-16] and SP (Shot Peening).

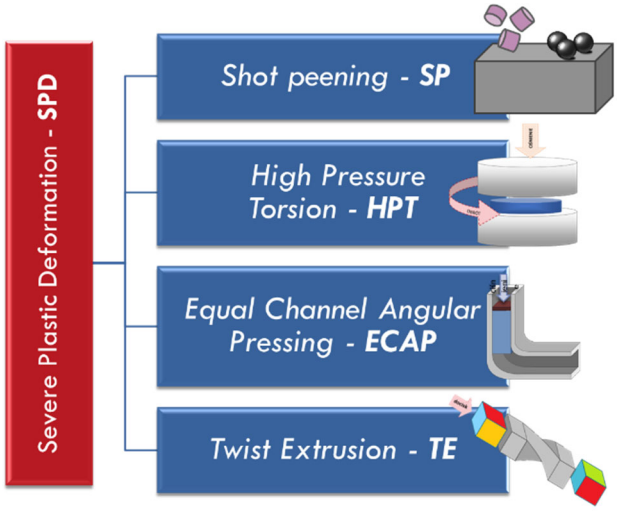

Fig. 1. SPD processing techniques

SPD methods are a set of techniques used to alter the microstructure of conventional materials into the ultra-fine structure of UFG (Ultra Fine Grain) and nanometric structure with grain sizes smaller than 100 nm.

The dislocation structure is reorganised (linear structure defects) due to subjecting the material to a very intensive forming process. This is possible only after exceeding the critical value of deformation – i.e., when the structure defects regroup, resulting in the formation of new cells, dislocation boundaries, and shear bands (narrow areas where intense shear strain is localised). The deformation must be much greater than in normal forming processes. This mechanism reduces the distance between grain boundaries and the diversity of their arrangement: increasing the angle of mutual inclination and twist of adjacent grains (the angles of twist and inclination of grain boundaries), which hinders dislocation movement and positively affects the mechanical properties of the material and its strength [17,18].

This research paper analyses twist extrusion (TE) – the extrusion process through a twisting channel. During the process, the sample is extruded through a channel consisting of two prismatic parts separated by a twist die ('twist area'). As the sample passes the twist area, the material is deformed and returns to its original shape after passing through the previous segment. The deformations produced during the TE process significantly change the material's microstructure, improving mechanical properties. The TE method is referred to as the three-dimensional version of the HPT method. The relevant variable parameters are:

- radius/distance between the sidewall of the channel and its R axis;
- total twist angle χ of the channel;
- length L of the twisted section.

Another important parameter is the angle between the die axis and the tangent of the channel twist. This angle, marked as β, depends on the other geometric features [19]:

$$\tan\beta = \frac{\chi * R}{L} \quad (1).$$

The following processes are present during twist extrusion: vortex-like flow with a large strain gradient, stretching and mixing metal particles. There are two shear planes during deformation. One of them is perpendicular, and the other is parallel to the specimen axis [15]. Many experiments have been carried out to understand the mechanism of deformation induced by strain during the TE process for various materials – including, but not limited to, aluminium and its alloys.

The influence of the number of MCSTE (Multi-channel Spiral Twist Extrusion) passes on the mechanical behaviour, and microstructural evolution of the AA1100 alloy was investigated in the research paper [20]. The results demonstrated that four MCSTE passes at a twist angle of 30° resulted in increased strength and hardness while maintaining elasticity. Metallographic observations indicated a 72% reduction in grain size compared to the original state.

The research paper [13] presented the extrusion process through a twisting channel using the Finite Element Method

(FEM). The influence of parameters such as backward pressure, loading, and friction on the stress and strain states, as well as the final shape of the workpieces, was investigated. The results showed that FEM simulation could provide an estimated value of backward pressure that can circumvent the possibility of creating shape defects in the workpiece. It has also been proven that using a low backward pres-sure can significantly improve die filling, which significantly impacts the distribution of plastic deformations. Simulations using a model with no friction or a low friction coefficient also result in the most uniform distribution of plastic deformations. The dominant shear stresses shaped the stress distribution achieved during the simulation near the transition planes.

In the research paper [21], a numerical simulation of the TE process was performed for the Ti-6Al-4V alloy. The influence of temperature and strain rate under high pressure on the material behaviour during the twist extrusion process was discussed. Additionally, the size of the accumulative distribution of strains and stresses, which determine the size of the final ultrafine grain (UFG – Ultrafine Grained) in the entire cross-section, was presented. The results showed that the maximal and minimal effective deformations are achieved in the corner and the centre of the sample, respectively. It was found that stress at the end of the twists of two passes is not equal to doubled strain from the first pass. The simulation results predict that the maximum values of plastic strains after 2-pass strains are 2.25 of the initial value. Research has also shown that not only does the von Mises stress and strain in the material vary from the center to the edge of the sample, but also that von Mises stress and strains vary along the extrusion direction.

The research paper [22] presents a simulation of three twist extrusions for commercially pure aluminium samples at ambient temperature. The results show that performing the next pass immediately after twist extrusion increases the shear strain magnitude in the centre of the specimen. High shear strain results in more grain refinement in the central regions of the sample in contrast to the corner ones.

In the research paper [23], to overcome the deformation inhomogeneity problem in SSE (Simple Shear Extrusion) and TE, a tandem process of SSE and TE (TST) was suggested. The authors used the finite element method to assess plastic deformation behaviour during the TST process. The results demonstrated that the TST process could produce relatively homogeneously deformed materials. The plastic deformation of the combined process is influenced by processing order and, therefore, the superposition of deformations and process synergy.

In the research paper [24], the crystallographic texture and microstructure of alloy AA6063 – after twist extrusion and subsequent cold rolling along and across the axis of twist extrusion – were investigated. The test results showed that each subsequent rolling in the direction across the axis of twist extrusion promotes the formation of texture-type brass. It was also noted that the texture grows from the centre to the periphery of the workpiece cross-section.

The research paper [25] utilised the alloy AA6063 and the TE forming process with backpressure after twist. The microhardness of alloy AA6063 was increased by about 40% by using post-twist back pressure compared to the initial conditions (twist extrusion without backpressure). Moreover, a relatively even microhardness distribution along the cross-section was observed.

Another example of a modification to the treatment of TE is to make a mould combining TE + ECAP = TCAP [14, 25-36]. As a result of the modification, the channel is bent after twisting, which makes the process much more efficient. The modification allows twisting and bending in one channel using three independent shear deformation paths, making the process more efficient in grain refinement and improving mechanical properties than ECAP [35]. In the second paper [36], the authors characterized in detail the effect of TCAP (twist channel angular press) treatment on the Al/Cu clad composite. For this purpose, they used experimental research as well as numerical methods. The deformation contributed to the deformation strengthening, causing an increase in the punch load by almost 50% and an increase in microhardness up to 130 HV for Cu wires, as well as an increase in temperature during machining. However, the second pass treatment temperature was still only ~37°C, which means that the treatment conditions were safe to introduce possible structural changes. In this work, simulations and experimental tests of the twist extrusion (TE) process were carried out on the RSA-501 alloy. Stress distribution, changes in the crystallographic texture, and hardness before and after the TE process are analyzed and discussed. Numerical analyzes allowed us to thoroughly check how the sample behaves during the TE process in any of its cross-sections. This made it possible to indicate places where the value exceeds the strength of the material, and thus the material cohesion is lost.

2. Materials and methods

2.1. Materials

The material subjected to forming processes must have appropriate properties that allow the use of this type of processing – otherwise, the structure will tear. Therefore, an experimental aluminium alloy with the trade name RSA 501 with the addition of magnesium, zirconium, manganese, and scandium was used in the research. Additions in the RSA 501 alloy, such as scandium and zirconium, allow for precipitation hardening and increase the recrystallisation temperature to 400°C – which affects the possibility of using

plastic deformations. On the other hand, magnesium significantly improves mechanical properties. As an alloying additive, manganese increases the strength of the moulded alloys, but plasticity usually decreases when it is in the form of undissolvable intermetallic compounds. Another equally important feature of manganese is the reduction of aluminium alloy resistance to stress corrosion and intercrystalline corrosion.

The properties of the investigated alloy are presented in Table 1. Its chemical composition was determined using the ARL™ PERFORM'X Sequential X-Ray Fluorescence Spectrometer, as shown in Table 2.

To achieve the maximum plasticity necessary to perform 'intensive' plastic formation processes, the alloy was annealed for 4 hours at a temperature of 500°C.

2.2. Method

Numerical analysis of the TE process

Samples made of RSA-501 aluminum alloy, dimensions: 8×10×35 mm, were used to simulate twists in an extrusion test through a twist channel. The die model used in the simulation was prepared based on the actual die (drawing of the die) used to perform the extrusion process through the twist channel.

For numerical analysis, it was assumed that the die twist channel is made from a rigid and nondeformable material, making it possible to analyse stress distribution without considering the phenomena occurring in the die. For numerical simulations of the TE process, the sample material was defined as an isotropic multilinear elastoplastic material based on the stress-strain curve (Fig. 2).

The numerical analysis examined the behaviour of the sample (Fig. 3) entering and papassinghrough the twist area up to the moment when the surface of the analysed sample was twisted at an angle of 90°. The sample was discretised using 2,800 elements and 13,437 nodes. The mesh size was selected to ensure a sufficient solution time with relatively little change in stress within the model. Numerical analysis was performed using ANSYS software.

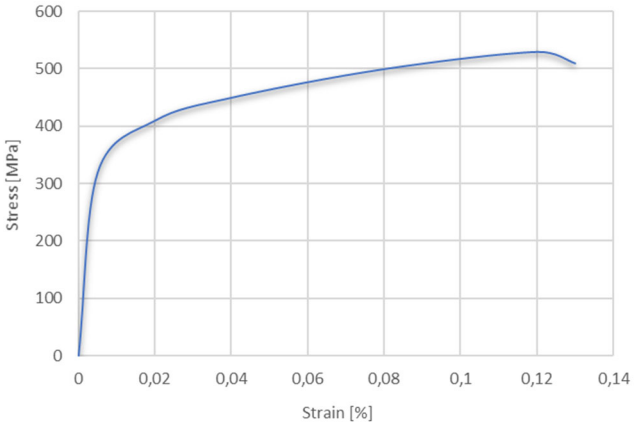

Fig. 2. True stress-strain curve

The pressure was applied to the sample to achieve an extrusion speed of 0.25 mm/s. The contact between the sample and the die was defined as frictional. Dynamic friction was set at 0.08, and static friction at 0.05. The channel angle Θ = 90° was also adopted as one of the boundary conditions.

Table 1.
RSA-501 material properties [1]

	Alloy name	RSA-501
	Condition at delivery	'AE – alternate extrusions' Cold extrusion using centrifugal extrusion
	Composition	Al Mg5 Mn1 Sc0.8 Zr0.4 (Scalmalloy)
Physical properties	Density, g/cm^3	2.65
	Thermal expansion, 10^{-6}/K	23
	Young's modulus, GPa	70
	Thermal conductivity, W/m.K	140
Mechanical properties	Tensile strength, MPa	575
	Yield point, MPa	525
	Elongation, %	12
	Hardness, HB	160
	Fatigue strength, MPa	400

Table 2.
Alloy chemical composition – author's research

Al	Mg	Zr	Mn	Sc	Fe	Si	Zn	Ga	Other
92.72	4.73	0.93	0.85	0.6	0.10	0.09	0.02	0.01	0.07

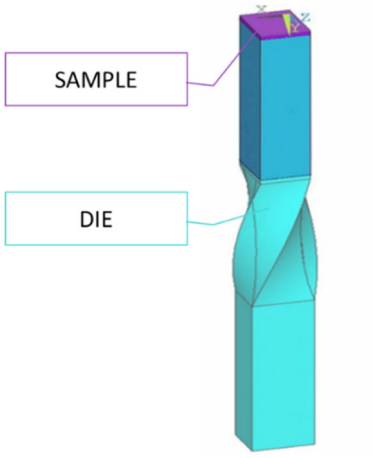

Fig. 3. Geometric and numerical model of the sample and TE die

Experimental verification of the TE process

A specially prepared die with a Θ = 90° channel angle was used to perform the extrusion test using the Twist Extrusion method (Fig. 4). Two samples made of RSA-501 aluminium alloy were extruded through the twist channel of the die, though only the first of them passed completely through the twist area. The samples were extruded using a special pis-ton rod, the pin of which enters the twist channel.

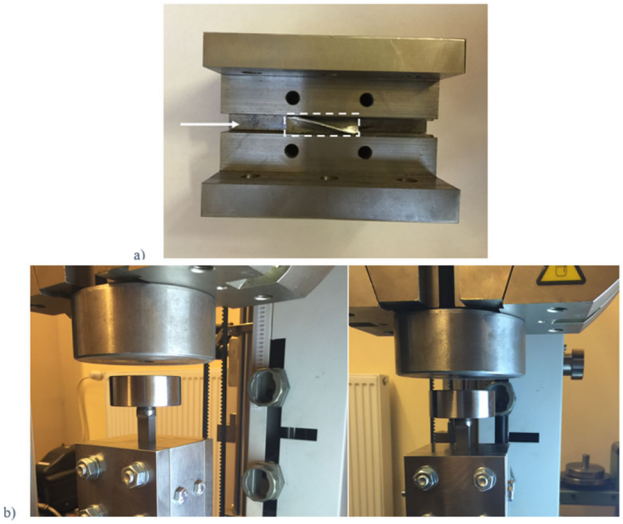

Fig. 4. A central part of the die with the sample-extrusion test

Samples with a prismatic cross-section of 8x10 mm and a length of 35 mm with the exact dimensions as in the numerical analysis were used.

To push the sample completely through the twist area and prevent deformation of the piston rod shaft, which is used to move the sample through the die, it was necessary to use two samples for one extrusion test, so the second test specimen remained in the twist area (as shown in Fig. 4b). This means that the first sample must pass completely through the twist area. In contrast, the piston rod shaft should remain in the first part of the twist channel (the second sample, located between the piston rod and the first sample, remains in the twist area).

Picture of the samples used for the Twist Extrusion process are shown in Figure 5. The sample at the bottom is the sample that entered the twist channel first and was twisted entirely up to 90°. The 'upper specimen' was only used to push the first specimen through the twist channel ultimately.

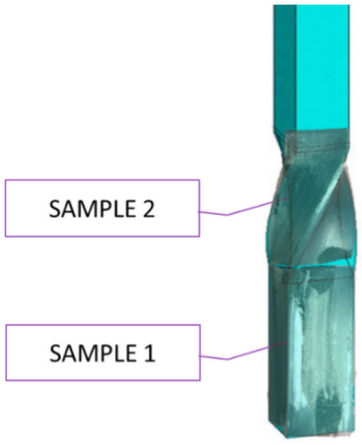

Fig. 5. Samples used for the TE process

Figure 6 shows the relationship between the force applied to the sample and piston movement. As seen in the graph, the force breaks when the piston is displaced 26-29 mm from the starting position when the front of the sample reaches the exit of the twist channel (i.e., it will soon leave the twist channel area). At the same time, after passing 30 mm, the front of the sample leaves the twist channel and completes the twist extrusion process. When the piston movement exceeds 35 mm, the second sample enters the twist channel and twists.

Residual stress measurements using a modified $\sin^2 \psi$ X-ray method

The residual stress measurements were performed using the X-ray method with the PROTO iXRD diffractometer. The following parameters were used for the test: Cr lamp, Kα1, 20 kV lamp voltage, 4 mA lamp current, Bragg angle 156.3° (reflections from the 222 surface family), the beta angle oscillation was 3°, LPA corrections and 2 mm aperture. The position of the diffraction peaks was approximated using Cauchy's formula. The elastic constants were adopted according to the software database: (1/2) S2 = 18.56·10–6 1/MPa and S1 = 4.79·10–6 1/MPa.

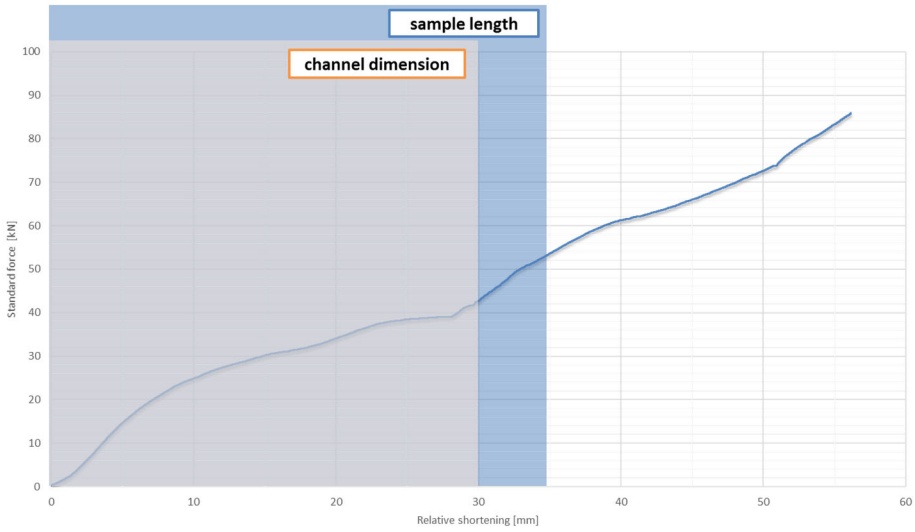

Fig. 6. Graph for the sample extruded through the die

Sample texture analysis

The pole figures were investigated with a PANalytical Empyrean X-ray diffractometer. The primary beam was a lamp with a Co anode (λ = 1.79Å) with an X-ray lens emitting a parallel beam with a divergence of 0.3°. The beam was limited to 2x1 mm using a cross collimator.

Figure 7. shows the sample's cut pattern and measurement planes after the TE process – marked in blue.

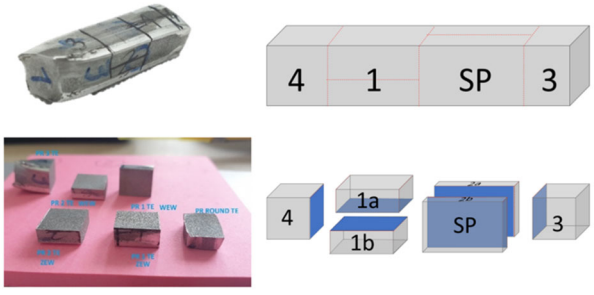

Fig. 7. Measurement surfaces – marked in blue

Fig. 8. Sample mounted on a goniometer stage during texture examination

The sample was mounted on a five-axis stage (Fig. 8). The scattered beam fell on a 0.18° parallel collimator, a 0.04 rad soller aperture and a proportional detector.

The Orientation Distribution Function (ODF) was calculated from the polar figures for the {111}, {200} and {220} surface families using the X'Pert Texture software. LaboTex software was also used for data analysis to determine texture components and their volume share.

Hardness measurement

Hardness measurements were made using the Vickers method on a KB Prüftechnik GmbH microhardness tester, following the PN-EN ISO 6507 standard. The samples were sand-papered with grades up to 1,000. Measurements were made in four consecutive stages of sample extrusion (Fig. 9):

1. Front of an untwisted sample;
2. Start twisting;
3. Final stage of twisting;
4. After the transition to the straight output channel. The final stage of extrusion.

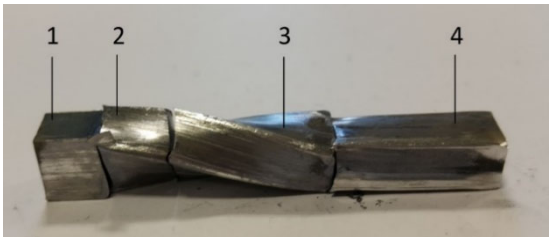

Fig. 9. Stages of sample extrusion

Each cross-section was examined in nine places, which resulted in obtaining the hardness distribution over the entire

sample cross-section (Fig. 10). The measurement for each point was repeated five times in an adjacent area to average the results.

Fig. 10. Sample cross-section with marked measurement points

The hardness measurements were made at a distance of about 1 mm from the sample edge, with an interval of about 4 mm along the 10 mm side (marked as X) and with an interval of 3 mm along the 8 mm side (marked as Y).

3. Results

3.1. Results of the TE process numerical analysis

Figures 11,12 shows the stress distribution on the sample surface during the extrusion process through a twist channel. The analysis was performed on the sample entering and passing through the twist area until the sample base was completely twisted. As shown in Figures 11,12, when the sample passes through the twist area, the stress is around 341 MPa and appears almost everywhere on the sample surface.

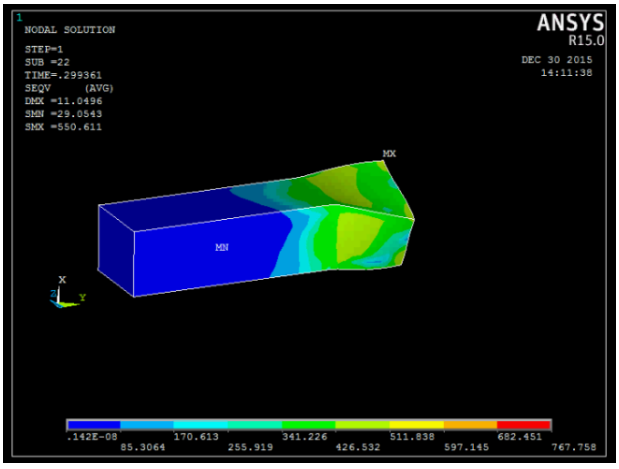

Fig. 11. Sample passing the twist area

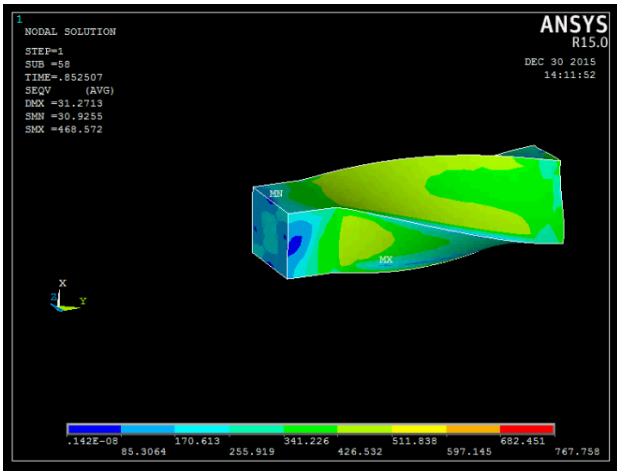

Fig. 12. Sample in the twist area

As seen in Figure 13, the highest stress (about 600 MPa) appears at the peaks of the front surface (Fig. 13 – Point 2) when exiting the twist area. Secondary hardening likely occurs at this point caused by the sample exiting the twist area. It is significant that stress of approx. 170 MPa begins to appear when the sample enters the twist area, as shown in Figure 13 – Point 1.

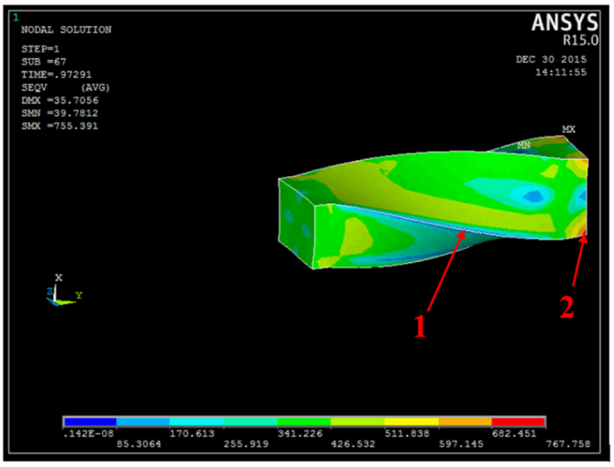

Fig. 13. Sample exiting the twist area

Figure 14 shows a schematic of the planes against which the sample stress during the TE process (i.e., at the entry to the twist channel) during the passage through the channel and at the exit from the channel were analysed. As visible in Figure 15, the stress distribution in the sample cross-section and stress values varied and depended on the stage of the twisting process to which the surface was subjected. Higher stress values at the edges of the specimen are caused by friction (deformation) of the material against the die surface.

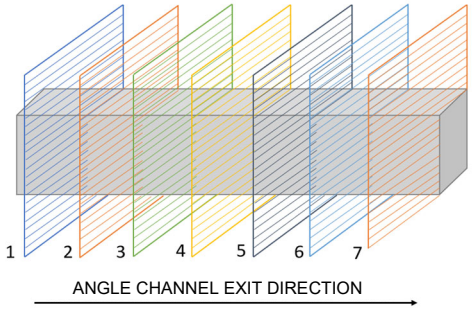

Fig. 14. Schematic of the analysed surface

The lowest stress values were observed in the centre part of the cross-section (Fig. 15), i.e., in the centre of the twisted specimen, along the twist plane (section 3-6, Fig. 14), before and just after twisting the specimen at an angle of 45° and ranged from 28 to 64 MPa.

Figure 16 shows the stress distribution in the sample (on the cross-sectional plane, parallel to the sidewall of the sample, and passing through its centre according to the schematic shown in Fig. 17) in relation to the step of the twist process in which the sample was subjected.

Due to the cross-sections presented in the drawings (Fig. 16), it is clearly visible that the highest stress values (approx. 420 MPa) appear on the surface 'entering' (right side of the sample) into the twist channel. When analysing the stress distribution on the sample surface, it is also noticeable that the highest stress values appear on the outer edges, which are subject to the strongest deformation processes.

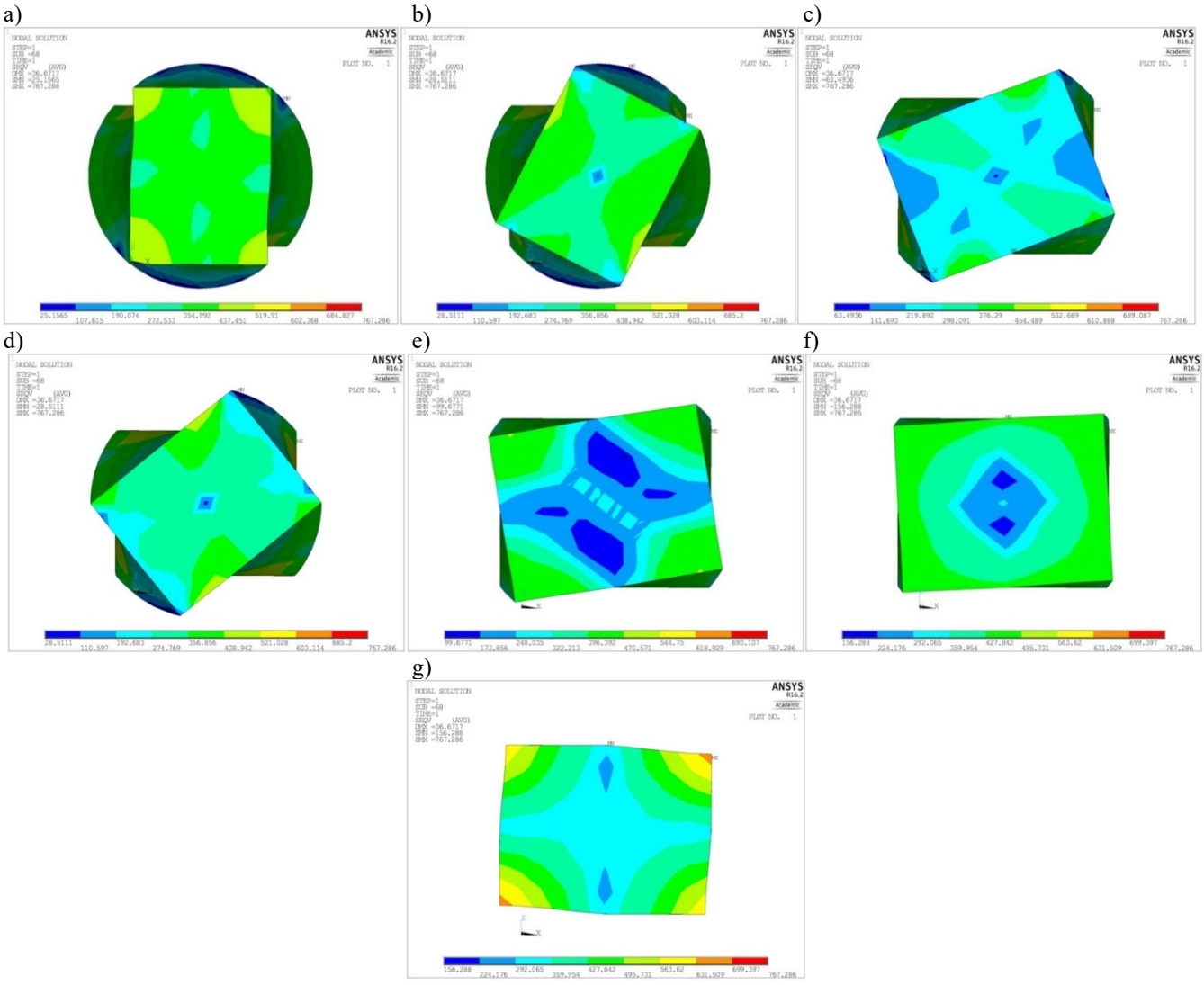

Fig. 15. Stress distribution on successive sample cross-sections during the TE process as shown in Figure 14 (1a-7g)

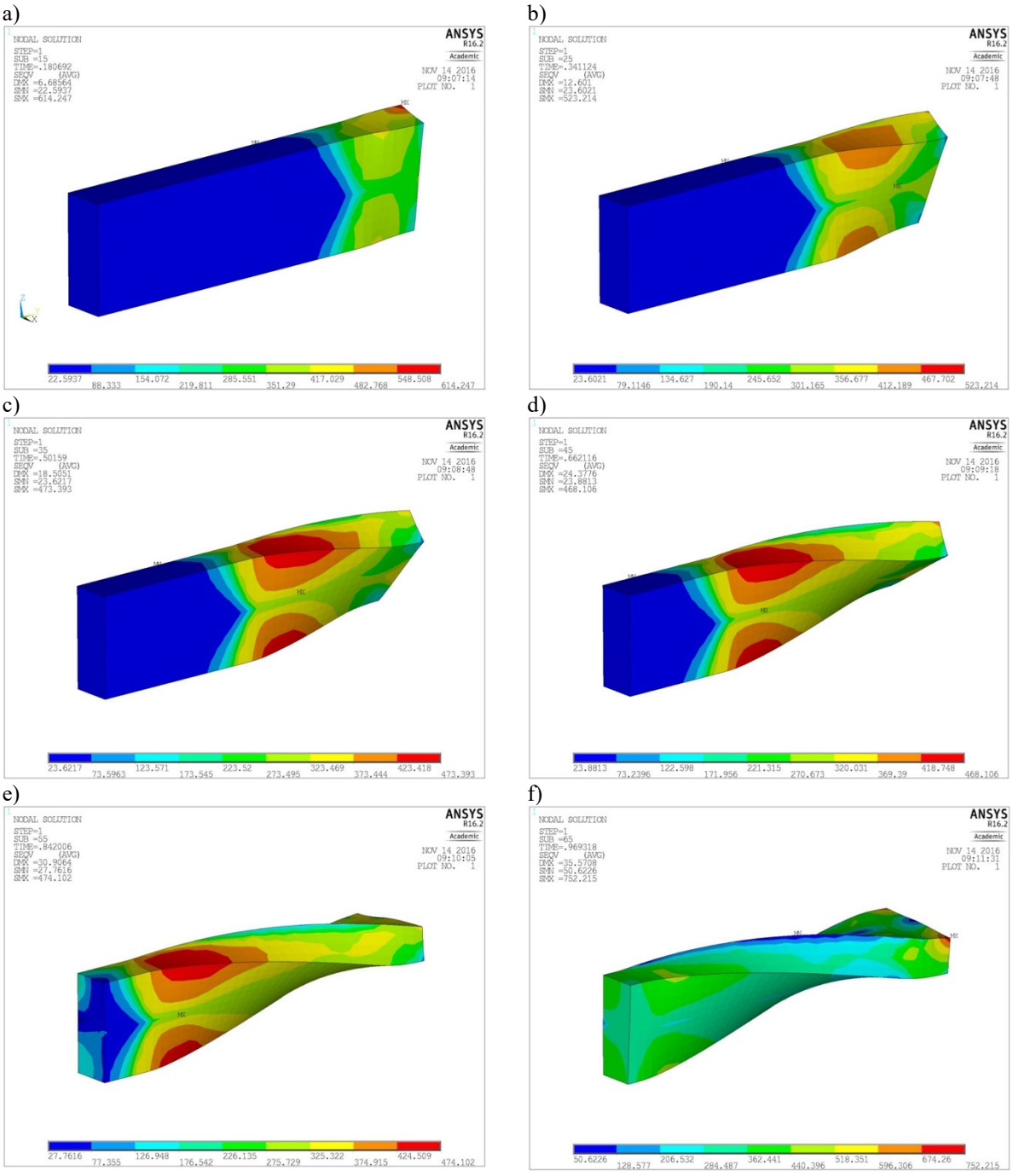

Fig. 16. Distribution of reduced stress on the surface on successive sample cross-sections (a-f) for successive time intervals

The lowest stress values occur along the axis through the centre of the specimen, parallel to the direction in which the specimen is extruded, as this area is subject to the weakest deformations.

The stress analysis on the surface of the cross-section and longitudinal section of the sample, as well as on its outer surface, shows that the highest stress values appear at the peaks of the sample front surface (cross-section peaks) when the sample exits the twist area (value approx. 630 MPa).

As stated above, this phenomenon is due to material hardening. The lowest stress values occur in the central part of the sample (the closer to the centre, the lower the stress because the central part of the sample is subjected to the weakest twisting).

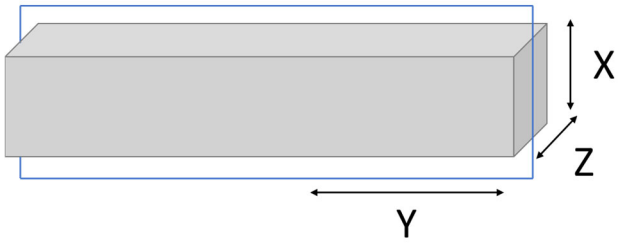

Fig. 17. Schematic of the analysed surface

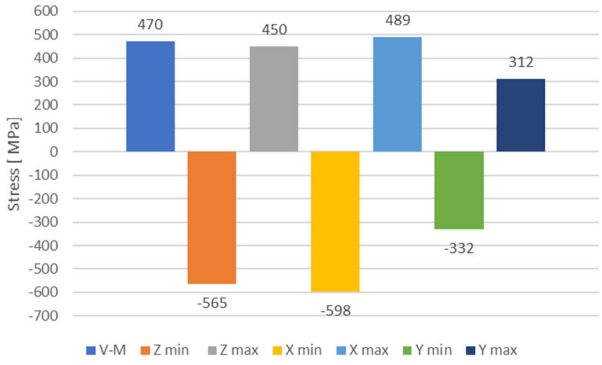

Fig. 18. Results of the numerical simulation of the TE process

Figure 18 summarises numerical analysis results for the TE process using a constant extrusion speed. The extrusion speed was chosen based on experimental tests in which the delamination of the material occurred above 0.25 mm/s, which proves that tensile strength was exceeded.

3.2. Results of experimental tests (residual stress)

Figure 19 shows the residual stress measurement points with the measurement directions marked. Figure 20 shows the directional stress distribution map obtained from the TE process numerical analysis. Figure 21 compares the results obtained from the experimental studies of the TE process with the results obtained using numerical analyses using the FEM method.

The experimental results show that stress values depend on the measurement point; at the same time, the highest stress values occur at the back of the sample (P6 – Fig. 19) that exits the channel. In the centre of the sample, there are significant differences in stress levels depending on the surface (edges of the sample) – which is typical for this type of process. The lowest stress values occur in the front of the sample, which enters the twist channel first and undergoes deformation, where the largest amount of lubricant is in the die.

Fig. 19. Schematic and designation of the analysed surfaces

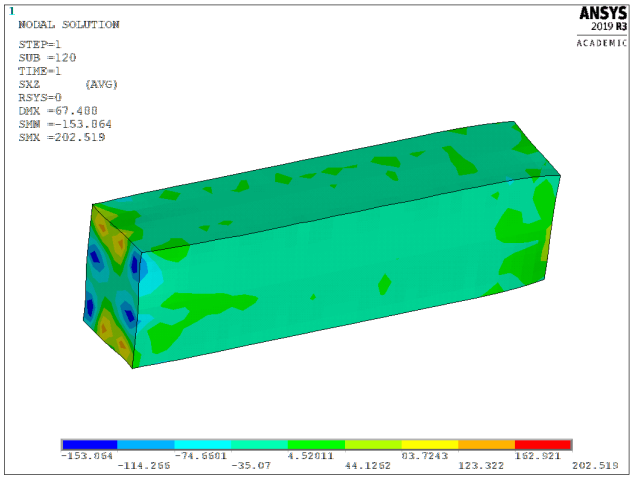

Fig. 20. Directional sample stress after the TE process

A comparison of the results with the FEM analysis shows that the stress values are more homogeneous in the numerical solution on the sample surface. It results from the unchanging boundary conditions used (friction coefficient) during the analysis.

3.3. Hardness test results

Figure 22 show the hardness measurements for the samples after the four consecutive stages of sample extrusion (Fig. 9). The measurement points have been described following Figure 10.

An increase in hardness can be noticed during the analysis of subsequent samples. The first sample (Fig. 22) showed a slight strengthening and increased hardness compared to the sample before the process. The sample no. 1 has not undergone the TE process. The change in parameters resulted from the pressure of the press – the compression. In Samples 2, 3, and 4 (Fig 22), hardness increases directly from the TE process. The highest hardness values were measured at the edges – measurement points 1,3,7,9.

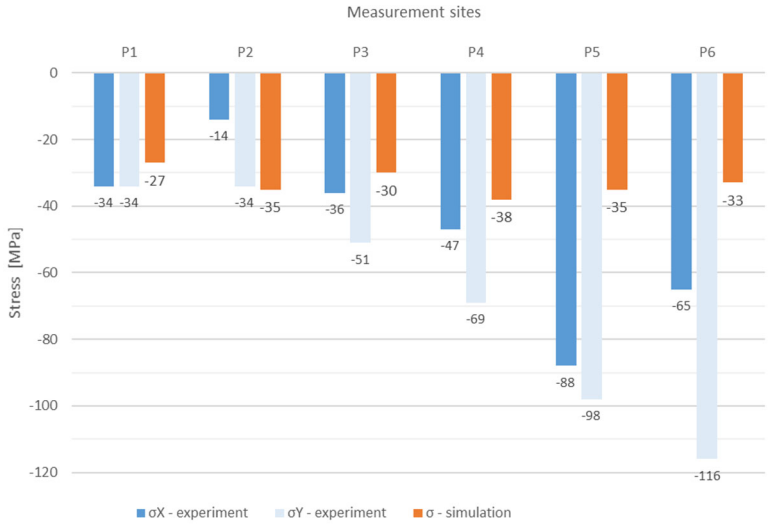

Fig. 21. Stress measurements for the experiment and simulation, made in six measurement points, shown in Figure 20

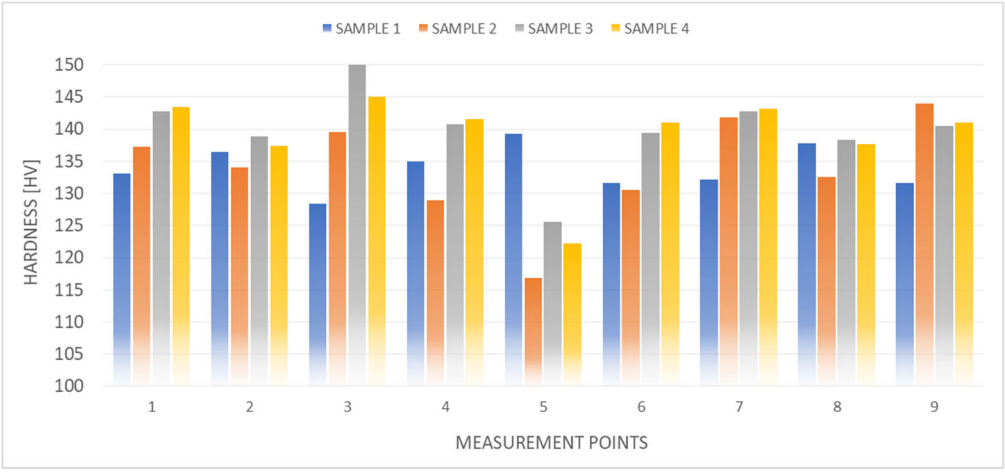

Fig. 22. Hardness distribution [HV]. Measurement points in relation to Figure 10

The observed stress distribution results from large local deformations of the sample in those places – the longest radius from the die axis. The opposite is point 5. The sample without treatment has the highest hardness value because treatment of TE in the core introduces texture with a relatively low background level (approx. 49%). The textures formed after the SPD processes result from grain rotation due to the deformation process. As a result, a specific crystallographic direction is parallel to the axis in the deformed polycrystalline material.

3.4. Crystallographic texture

Below is a comparison of the diffractograms (Fig. 23) obtained in conditions of symmetrical geometry of a deformed and undeformed sample. There are clear differences in the ratio of the reflection intensity and, for the deformed sample, a very weak reflection for the angle 2Theta = 77°.

Reference sample (before the SPD process)

The volume fraction, orientation distribution functions (Fig. 24), and pole figures (Fig. 25) for the initial samples (samples after normalisation at 500°C for 4 hours) before being subjected to intensive forming processes are presented below. Figure 24 shows the share of individual texture components in the tested sample. Based on the analysis, it can be concluded that the texture in the initial/reference sample is very poorly developed, as evidenced by the high background level of 79%. The axial texture components are at a low level – <001> and <110> occupy 2% of the sample.

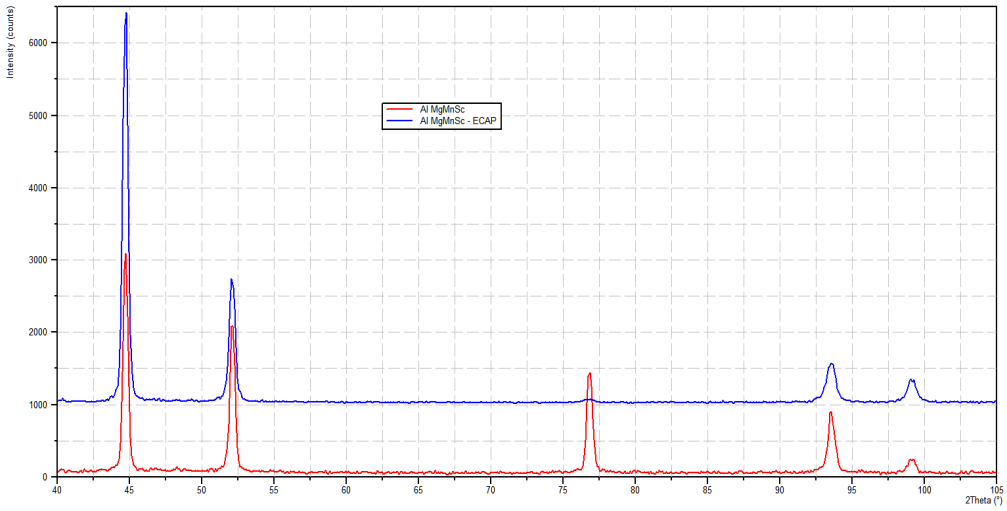

Fig. 23. Diffractogram for a reference sample and a sample after the ECAP process

Component designation {hkl} <uvw>	Component volumetric fraction [%]	Orientation distribution functions for a sample „ befor TE”
{110} <1$\bar{1}$1>	3	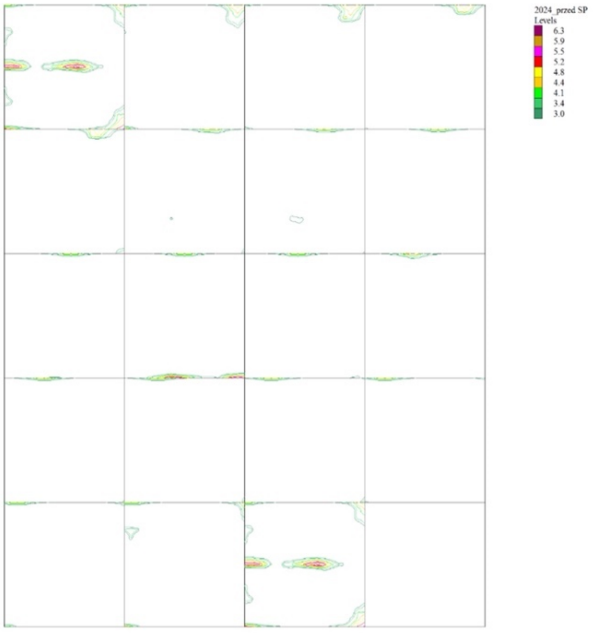
{110} <001> -goss	4	
{001} <100> - cube	1	
{112} <11$\bar{1}$> - C	6	
{025} <100>	1	
{011} <6$\bar{7}$7> ~{001} <1$\bar{1}$1>	0	
<001>	2	
<110>	4	
Tło	79	

Fig. 24. The volume fraction of the main texture components in the tested samples and the orientation distribution functions

Figure 26 shows the Orientation Distribution Functions (ODF) and summarises the shares of individual texture components for all measurement surfaces of the tested sample and the polar figures obtained from individual samples in Figures 27-32.

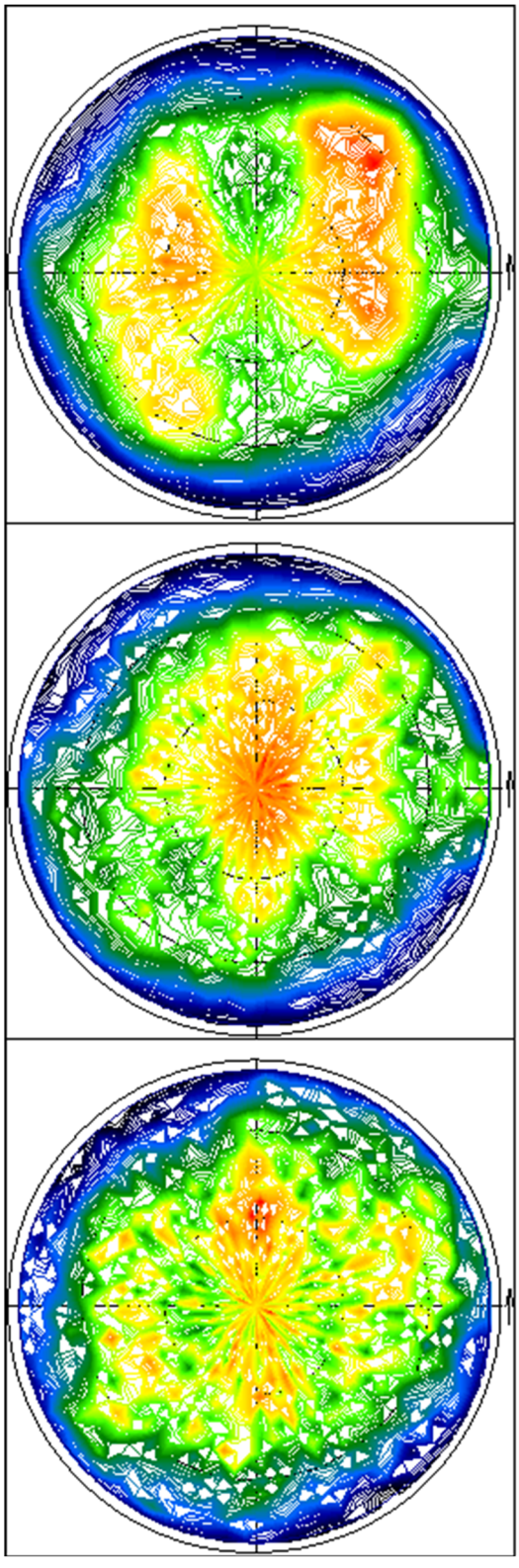

Pole figure: 111 Corr.
2Theta: 44.7000
Intensities:

	Psi	Phi	Intesity
Min	85.0	92.5	0.000
Max	55.0	42.5	1253.160

Dimension: 2D
Projection: Schmidt
Scale Linear
Color maps: X'Pert

Pole figure: 200 Corr.
2Theta: 52.1000
Intensities:

	Psi	Phi	Intesity
Min	85.0	92.5	4.840
Max	0.0	32.5	556.960

Dimension: 2D
Projection: Schmidt
Scale Linear
Color maps: X'Pert

Pole figure: 220 Corr.
2Theta: 76.7000
Intensities:

	Psi	Phi	Intesity
Min	85.0	122.5	1.210
Max	35.0	87.5	228.010

Dimension: 2D
Projection: Schmidt
Scale Linear
Color maps: X'Pert

Fig. 25. Pole figures for the sample before the SP process

Component designation {hkl} <uvw>	Component volumetric fraction [%]	Orientation distribution functions for a sample „ befor TE”
sample 2b		
{110} <1$\bar{1}$1>	4	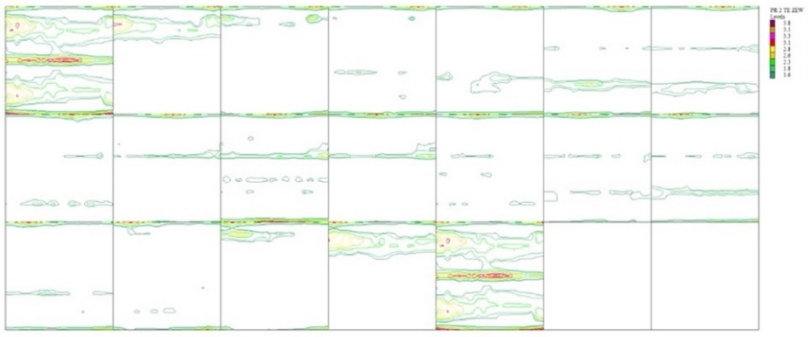
{001} <100>	6	
{11$\bar{2}$} <111>	6	
{110} <1$\bar{1}$2>	3	
{110} <001>	2	
{3$\bar{8}$5} <111>	4	
{013} <100>	14	
Tło	61	
sample 2a		
{110} <1$\bar{1}$1>	4	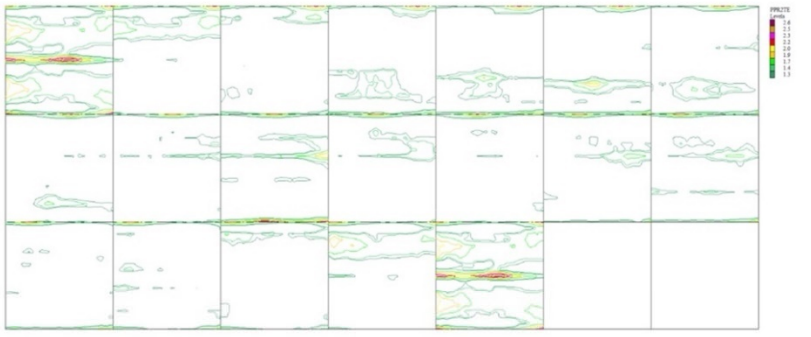
{001} <100>	5	
{11$\bar{2}$} <111>	4	
{110} <1$\bar{1}$2>	1	
{110} <001>	0	
{3$\bar{8}$5} <111>	3	
{013} <100>	5	
Tło	78	
sample 3		
<100>	4	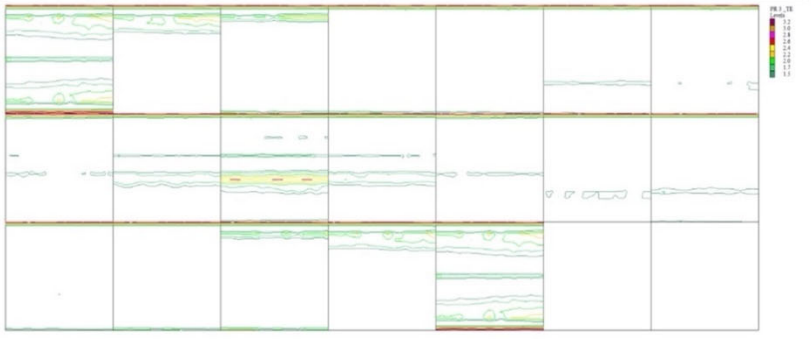
<111>	2	
{111} <$\bar{4}$13>	5	
Tło	89	

Fig. 26. The volume fraction of the main texture components in the tested samples and the orientation distribution functions

Component designation {hkl} <uvw>	Component volumetric fraction [%]	Orientation distribution functions for a sample „ befor TE”
sample 4		
<100>	7	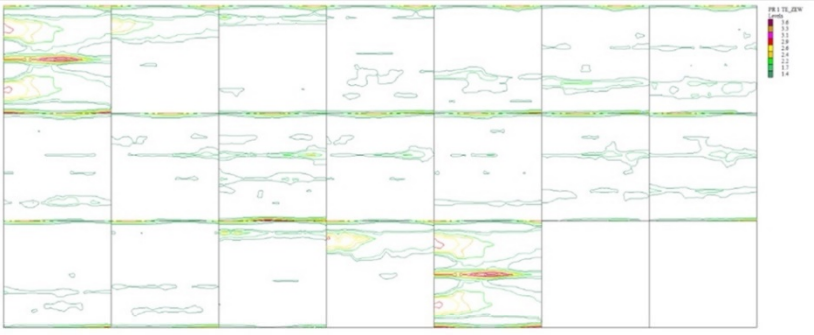
<111>	6	
{111} <$\bar{4}$13>	2	
Tło	85	
sample 1b		
{110} <1$\bar{1}$1>	13	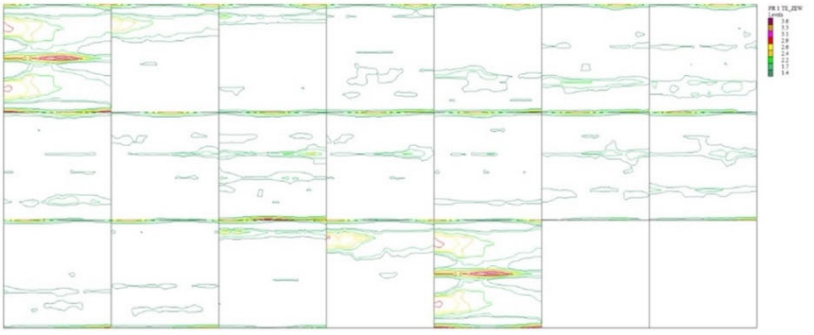
{001} <100>	8	
{11$\bar{2}$} <111>	15	
{110} <1$\bar{1}$2>	2	
{110} <001>	1	
{3$\bar{8}$5} <111>	0	
{013} <100>	12	
Tło	49	

Fig. 26. *cont.* The volume fraction of the main texture components in the tested samples and the orientation distribution functions

The 2a, 2b, and 1b sample surfaces have similar textures (i.e., the generated deformation leads to forming the same components). Comparing the intensity of individual components on the ODF scale, it can be concluded that stronger textures developed in surfaces 1b and 2b. However, comparing the texture level of the tested volume in samples 2a and 2b, it can be seen that a higher texture level was achieved in sample 2b (background at 61%). Samples 3 and 4 developed a similar fibrous texture. Sample 1b was the most textured, with a background level of 49%.

4. Summary and discussion of the results

An analysis of the TE process for the RSA-501 alloy was performed for this research paper. The process consisted of extruding the material through a twist channel with a twist area where an element was twisted (in this case, by 90˚). As a result, the tested material achieved more favourable strength properties and increased its hardness.

By analysing the stress distribution on the surface of the sample after the TE process, it can be noted that the highest stress values appeared on the outer edges, which are subject to the strongest deformation processes (Figs. 12,13). In contrast, the lowest stress values occurred along the axis passing through the centre of the sample, parallel to the direction of sample extrusion, because this area is subject to the least amount of twist. This is also confirmed by the results presented in the available literature on the TE process for various materials [14,21,25, 29-31]. However, the observed differences in stress values are caused by different boundary conditions of the TE process.

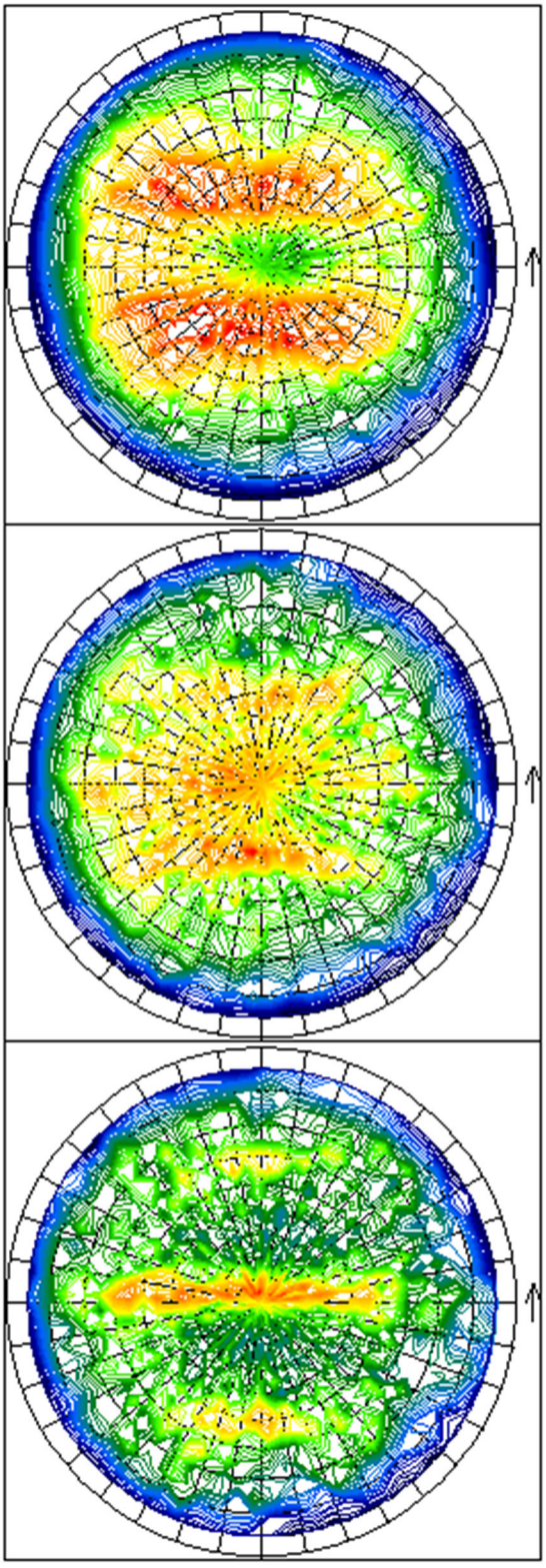

Pole figure: 111 Corr.
2Theta: 44.7000
Intensities:

	Psi	Phi	Intesity
Min	85.0	247.5	43.560
Max	30.0	242.5	576.000

Dimension: 2D
Projection: Wulff
Scale Linear
Color maps: X'Pert

Pole figure: 200 Corr.
2Theta: 52.1000
Intensities:

	Psi	Phi	Intesity
Min	85.0	237.5	24.010
Max	30.0	262.5	268.960

Dimension: 2D
Projection: Wulff
Scale Linear
Color maps: X'Pert

Pole figure: 220 Corr.
2Theta: 76.7000
Intensities:

	Psi	Phi	Intesity
Min	85.0	137.5	8.410
Max	5.0	102.5	151.290

Dimension: 2D
Projection: Wulff
Scale Linear
Color maps: X'Pert

Fig. 27. Pole figures after the TE process – Sample 2a

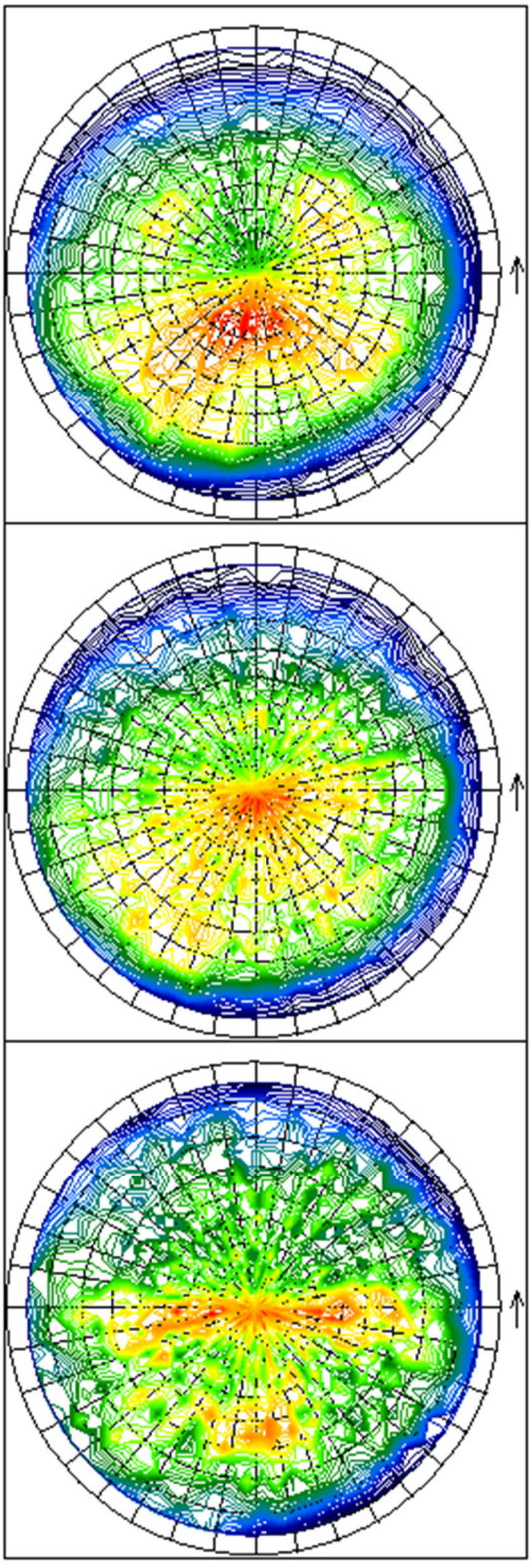

Pole figure: 111 Corr.
2Theta: 44.7000
Intensities:

	Psi	Phi	Intesity
Min	85.0	32.5	3.610
Max	20.0	257.5	600.250

Dimension: 2D
Projection: Wulff
Scale Linear
Color maps: X'Pert

Pole figure: 200 Corr.
2Theta: 52.1000
Intensities:

	Psi	Phi	Intesity
Min	85.0	37.5	0.000
Max	5.0	282.5	262.440

Dimension: 2D
Projection: Wulff
Scale Linear
Color maps: X'Pert

Pole figure: 220 Corr.
2Theta: 76.8000
Intensities:

	Psi	Phi	Intesity
Min	85.0	32.5	0.000
Max	5.0	332.5	127.690

Dimension: 2D
Projection: Wulff
Scale Linear
Color maps: X'Pert

Fig. 28. Pole figures after the TE process – Sample 2b

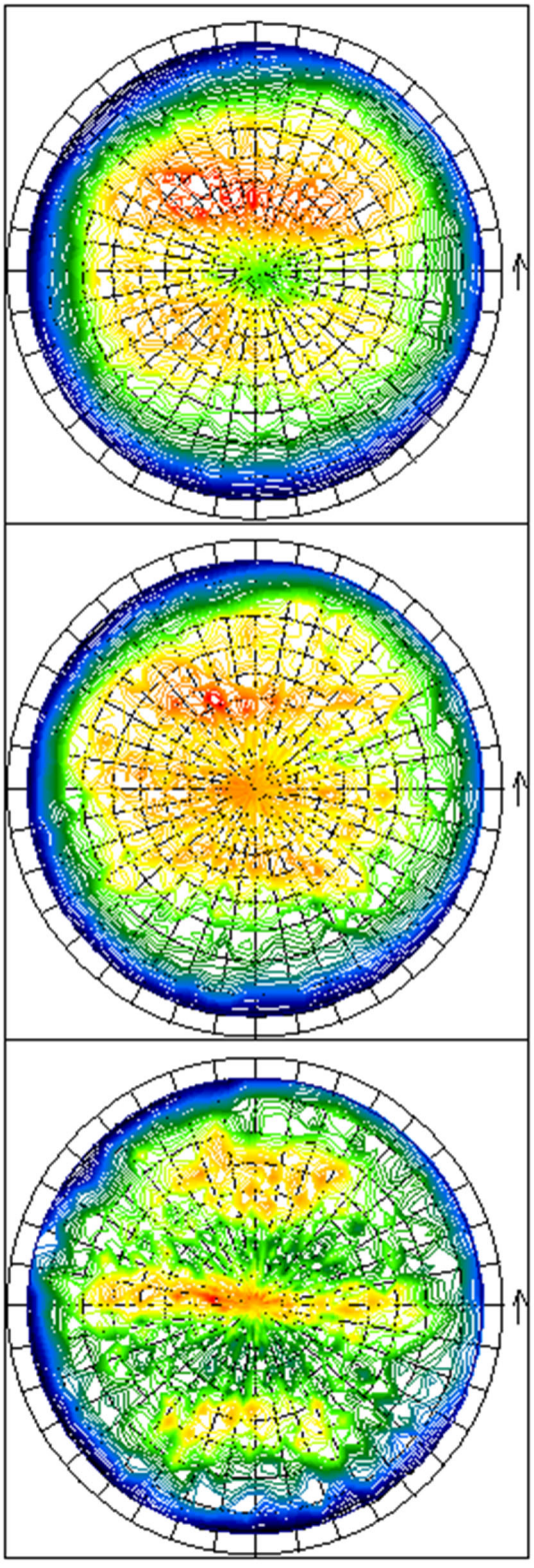

Pole figure: 111 Corr.
2Theta: 44.7000
Intensities:

	Psi	Phi	Intesity
Min	85.0	127.5	5.290
Max	30.0	92.5	1176.490

Dimension: 2D
Projection: Wulff
Scale Linear
Color maps: X'Pert

Pole figure: 200 Corr.
2Theta: 52.1000
Intensities:

	Psi	Phi	Intesity
Min	85.0	137.5	9.610
Max	40.0	112.5	501.760

Dimension: 2D
Projection: Wulff
Scale Linear
Color maps: X'Pert

Pole figure: 220 Corr.
2Theta: 76.7000
Intensities:

	Psi	Phi	Intesity
Min	85.0	137.5	0.000
Max	20.0	172.5	237.160

Dimension: 2D
Projection: Wulff
Scale Linear
Color maps: X'Pert

Fig. 29. Pole figures after the TE process – Sample 1a

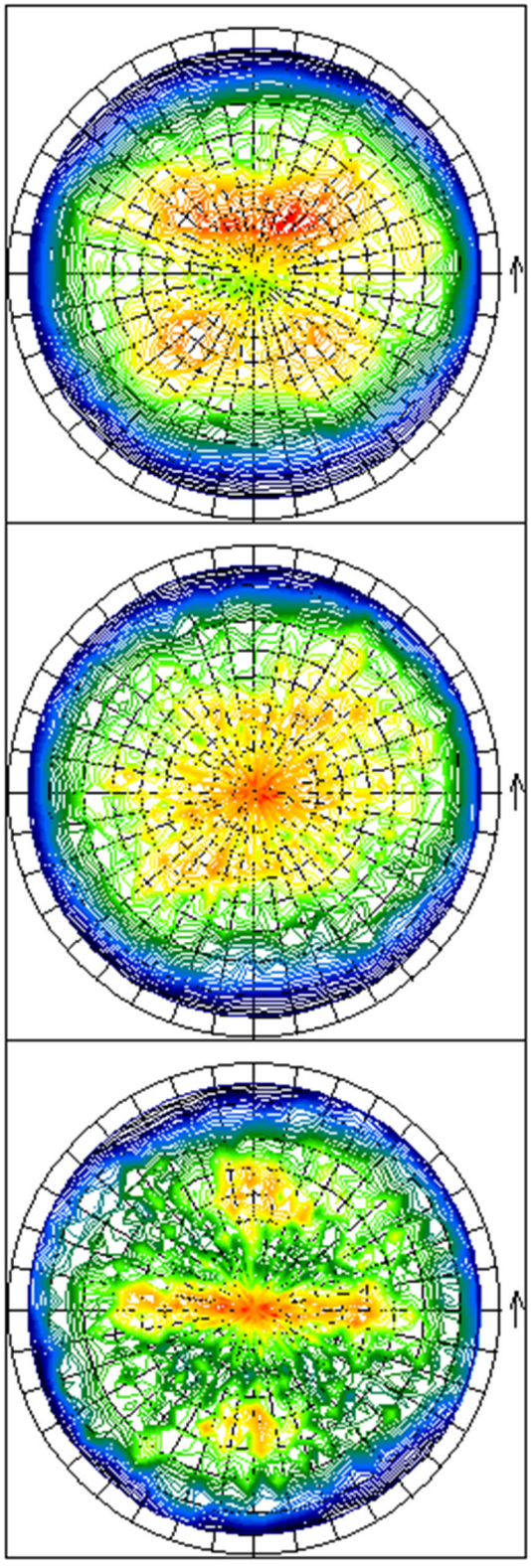

Pole figure: 111 Corr.
2Theta: 44.7000
Intensities:

	Psi	Phi	Intesity
Min	85.0	257.5	28.090
Max	30.0	57.5	1102.240

Dimension: 2D
Projection: Wulff
Scale Linear
Color maps: X'Pert

Pole figure: 200 Corr.
2Theta: 52.1000
Intensities:

	Psi	Phi	Intesity
Min	85.0	257.5	10.890
Max	0.0	57.5	479.610

Dimension: 2D
Projection: Wulff
Scale Linear
Color maps: X'Pert

Pole figure: 220 Corr.
2Theta: 76.7000
Intensities:

	Psi	Phi	Intesity
Min	85.0	92.5	0.000
Max	0.0	182.5	216.090

Dimension: 2D
Projection: Wulff
Scale Linear
Color maps: X'Pert

Fig. 30. Pole figures after the TE process - Sample 1b

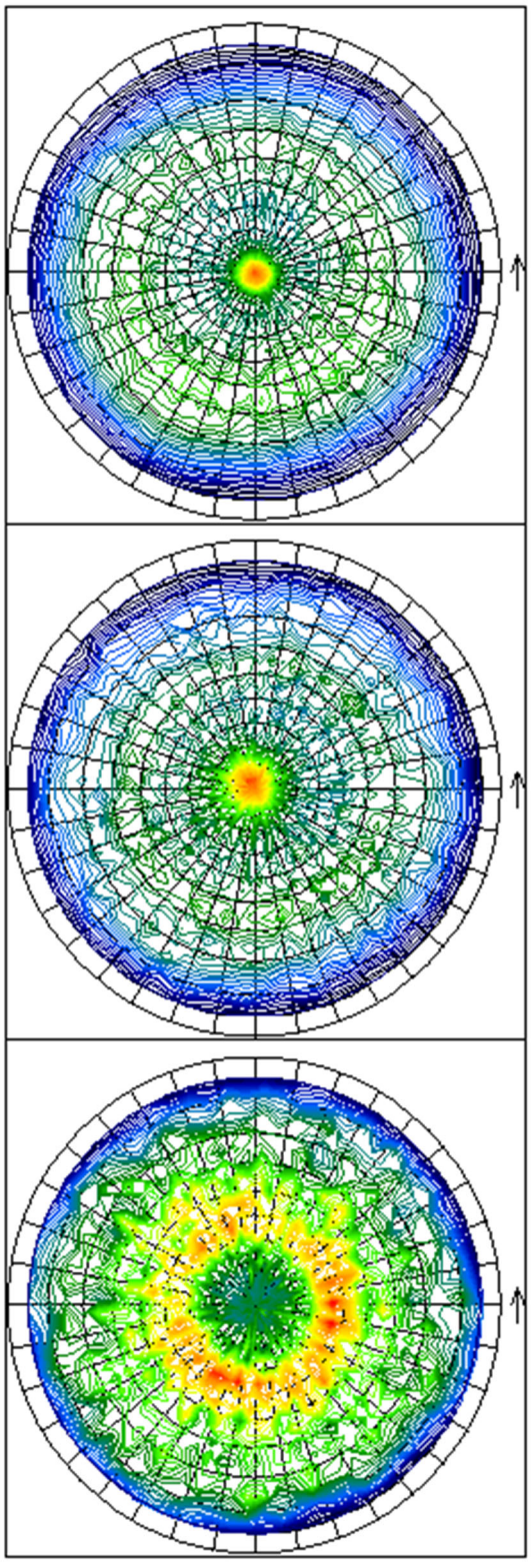

Pole figure: 111 Corr.
2Theta: 44.7000
Intensities:

	Psi	Phi	Intesity
Min	85.0	307.5	81.000
Max	0.0	242.5	1705.690

Dimension: 2D
Projection: Wulff
Scale Linear
Color maps: X'Pert

Pole figure: 200 Corr.
2Theta: 52.1000
Intensities:

	Psi	Phi	Intesity
Min	85.0	37.5	42.250
Max	0.0	272.5	767.290

Dimension: 2D
Projection: Wulff
Scale Linear
Color maps: X'Pert

Pole figure: 220 Corr.
2Theta: 76.7000
Intensities:

	Psi	Phi	Intesity
Min	85.0	317.5	0.000
Max	35.0	2.5	228.010

Dimension: 2D
Projection: Wulff
Scale Linear
Color maps: X'Pert

Fig. 31. Pole figures after the TE process - Sample 4

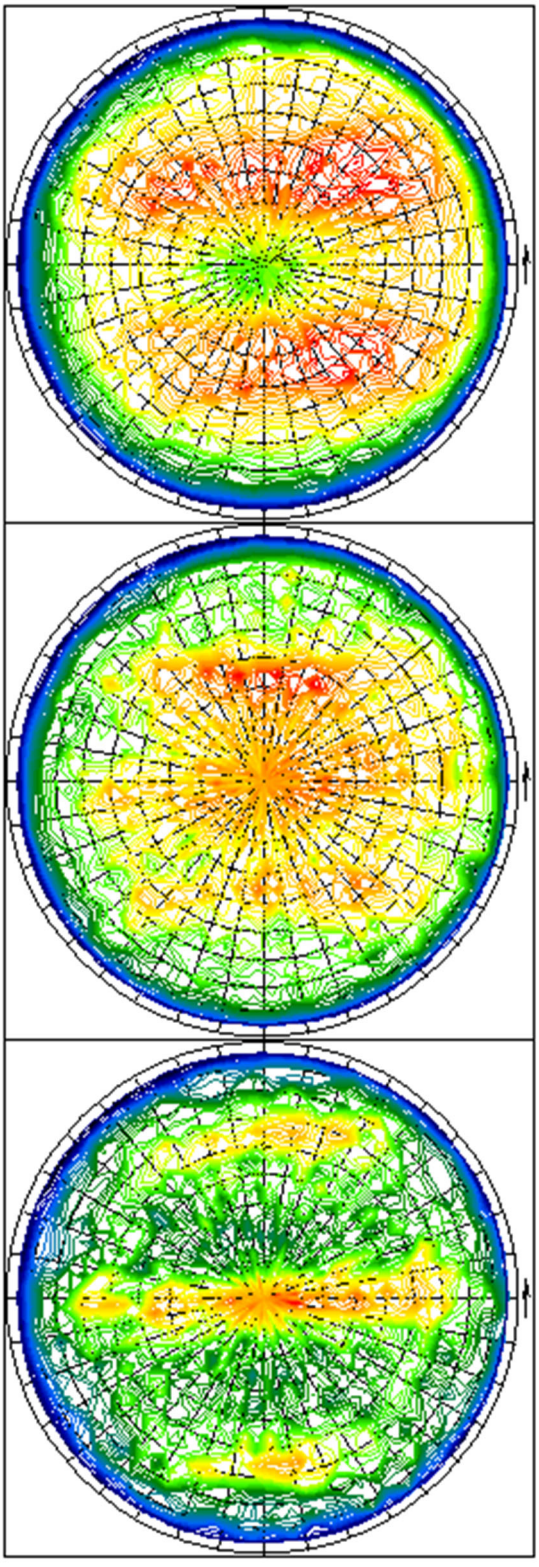

Pole figure: 111 Corr.
2Theta: 44.7000
Intensities:

	Psi	Phi	Intesity
Min	85.0	127.5	96.040
Max	45.0	307.5	985.960

Dimension: 2D
Projection: Schmidt
Scale Linear
Color maps: X'Pert

Pole figure: 200 Corr.
2Theta: 52.1000
Intensities:

	Psi	Phi	Intesity
Min	85.0	107.5	40.960
Max	35.0	62.5	466.560

Dimension: 2D
Projection: Schmidt
Scale Linear
Color maps: X'Pert

Pole figure: 220 Corr.
2Theta: 76.7000
Intensities:

	Psi	Phi	Intesity
Min	85.0	127.5	0.000
Max	10.0	352.5	246.490

Dimension: 2D
Projection: Schmidt
Scale Linear
Color maps: X'Pert

Fig. 32. Pole figures after the TE process – Sample 3

The effect of the changes in the texture is also confirmed by the obtained results of numerical analyses and the first hardness changes on the cross-section of the sample. The results showed that the maximum and minimum effective deformations are achieved in the corner and the centre of the sample, respectively.

The textures formed after the SPD processes result from grain rotation due to the deformation process. As a result, a specific crystallographic direction is parallel to the axis in the deformed polycrystalline material (in the case of products with an axial shape – e.g., wire, rods) or in the case of planar products (e.g., sheets). Compared to the reference sample with a background level of 79%, there was a significant increase in texture after the TE process, as the lowest background level for the post-TE samples was relatively low (at 49%).

Due to crystallographic structure texturing, it is possible to obtain new material properties – as evidenced by many publications [32, 34-36]. These publications show that similar texture components were obtained during experimentation. Based on the article [37] in which slow-speed extrusion was investigated, the paper's authors also consider conducting tests with variable process temperature. Because the results of the work [38] show that low-speed extrusion led to the improvement of the microstructure and a significant improvement of the mechanical properties. With the process, the temperature increased in the range of 350°C, 400°C, and 450°C; the mean z-are sizes of the extruded sheets were then ~2.7 μm, ~4.1 μm, and ~6.0 μm. The article's authors [39] noticed similar benefits of increasing the ambient temperature above the temperature to 200C for one of the SPD (TCAP) processes. The obtained results showed a significant influence of forming under these conditions on the formation of displacement substructure and its influence on tensile properties. Significant grain refinement was also noticed, depending on the number of passes through the material. Based on the results of microstructural analyses presented in this paper, it can be concluded that the strong plastic deformations caused by TCAP significantly impact grain refinement and increase strength properties while maintaining the plasticity of the tested alloy. Other authors also discussed reinforcing mechanisms such as grain grinding or cardboard modification and their impact on improving the matrices' strength properties [37, 40-42].

As polycrystalline engineering material is usually textured, a higher background value than in the reference sample may be because the nature of the texture is sometimes different – which, on the one hand, is a property of the material but, on the other hand, means that inhomogeneity has to be taken into account in the texture measurement analysis results and may lead to a situation where the texture measurement is not representative of the material or the tested technology. In the simplest case, when the material has the same texture throughout the entire volume, the material has a homogeneous texture. However, there are more cases when the texture of the material is inhomogeneous (i.e., not uniform across the entire volume), and the nature of this inhomogeneity may differ. Most often, it depends on the object's geometry and production technology. Additionally, the texture is a statistical property and is based on the presence of privileged crystallographic orientations in a multielement polycrystalline aggregate. Those differences can be observed in the texture of the surface layers of the product and its internal layers. However, it should be remembered that the texture may influence the elasticity, creep strength, fatigue resistance, and corrosion resistance. The increase in hardness was obtained by breaking the grains of the material. At the same time, the samples – after passing through the channel – retain their original dimensions (there is only a slight rounding at the edges).

It should also be noted that microhardness increases due to the TE process. The largest values were observed at the edges; a similar nature of the distribution was obtained by Nouri and his team [27]. This phenomenon is confirmed by the results of the numerical simulation presented in this paper, in which the highest stress values were obtained near the edge and the lowest in its central part.

5. Conclusions

- It is possible to examine the spatial stress distribution on the technological surface layer as well as its redistribution during the TE process.
- Using numerical simulations, it is possible to determine potential locations of cracks and structure reinforcements in critical places – edges of the sample, and the stress value is 418 to 752 MPa.
- The stress nature during experiments is confirmed by the introduction of residual stress to the technological surface layer as a result of the TE process at a similar level as it was shown using numerical methods.
- The highest HV hardness values are at the edges of the sample – measurement points 1,3,7,9 for samples 2 and 3.
- The TE process led to strengthening – for the highest level of texture, the background was 49%.

References

[1] Z. Yan, J. Zheng, J. Zhu, Z. Zhang, Q. Wang, Y. Xue, High Ductility with a Homogeneous Microstructure of a Mg–Al–Zn Alloy Prepared by Cyclic Expansion Extrusion with an Asymmetrical Extrusion Cavity, Metals 10/8 (2020) 1102.
DOI: https://doi.org/10.3390/met10081102

[2] A. Azushima, R. Kopp, A. Korhonen, D.Y. Yang, F. Micari, G.D. Lahoti, P. Groche, J. Yanagimoto, N. Tsuji, A. Rosochowski, A. Yanagida, Severe plastic deformation (SPD) processes for metals, CIRP Annals 57/2 (2008) 716-735. DOI: https://doi.org/10.1016/j.cirp.2008.09.005

[3] B. Wan, W. Chen, T. Lu, F. Liu, Z. Jiang, M. Mao, Review of solid state recycling of aluminum chips, Resources, Conservation and Recycling 125 (2017) 37-47. DOI: https://doi.org/10.1016/j.resconrec.2017.06.004

[4] J.-K. Han, H.-J. Lee, J. Jang, M. Kawasaki, T.G. Langdon, Micro-mechanical and tribological properties of aluminum-magnesium nanocomposites processed by high-pressure torsion, Materials Science and Engineering: A 684 (2017) 318-327. DOI: https://doi.org/10.1016/j.msea.2016.12.067

[5] R. Kulagin, A. Mazilkin, Y. Beygelzimer, D.G. Savvakin, I. Zverkova, D. Oryshych, H. Hahn, Influence of High Pressure Torsion on structure and properties of Zr-Ti-Nb alloy synthesized from TiH_2, ZrH_2 and Nb powders, Materials Letters 233 (2018) 31-34. DOI: https://doi.org/10.1016/j.matlet.2018.08.139

[6] S.O. Rogachev, R.V. Sundeev, N.Y. Tabachkova, High pressure torsion-induced amorphous phase in a multilayer V-10Ti-5Cr/Zr-2.5Nb/V-10Ti-5Cr hybrid material, Materials Letters 234 (2019) 220-223. DOI: https://doi.org/10.1016/j.matlet.2018.09.112

[7] K. Edalati, Z.A. Horita, A review on high-pressure torsion (HPT) from 1935 to 1988, Materials Science and Engineering: A 652 (2016) 325-352. DOI: https://doi.org/10.1016/j.msea.2015.11.074

[8] B. Omranpour, L. Kommel, V. Mikli, E. Garcia, J. Huot, Nanostructure development in refractory metals: ECAP processing of Niobium and Tantalum using indirect-extrusion technique, International Journal of Refractory Metals and Hard Materials 79 (2019) 1-9. DOI: https://doi.org/10.1016/j.ijrmhm.2018.10.018

[9] V.M. Segal, Severe plastic deformation: simple shear versus pure shear, Materials Science and Engineering: A 338/1-2 (2002) 331-344. DOI: https://doi.org/10.1016/S0921-5093(02)00066-7

[10] R.Z. Valiev, Y. Estrin, Z. Horita, T.G. Langdon, M.J. Zechetbauer, Y.T. Zhu, Producing bulk ultrafine-grained materials by severe plastic deformation, JOM 58 (2006) 33-39. DOI: https://doi.org/10.1007/s11837-006-0213-7

[11] R.Z. Valiev, T.G. Langdon, Principles of equal-channel angular pressing as a processing tool for grain refinement, Progress in Materials Science 51/7 (2006) 881-981. DOI: https://doi.org/10.1016/j.pmatsci.2006.02.003

[12] J. Sawicki, J. Świniarski, M. Stegliński, P. Byczkowska, Numerical analysis of twist extrusion pressing of Al-Mg-Mn-Sc-Zr scalmalloy, Archives of Metallurgy and Materials 63/3 (2018) 1385-1392. DOI: https://doi.org/10.24425/123816

[13] M.I. Latypov, I.V. Alexandrov, Y.E. Beygelzimer, S. Lee, H.S. Kim, Finite element analysis of plastic deformation in twist extrusion, Computational Materials Science 60 (2012) 194-200. DOI: https://doi.org/10.1016/j.commatsci.2012.03.035

[14] U.M. Iqbal, V.S.S. Kumar, An analysis on effect of multipass twist extrusion process of AA6061 alloy, Materials and Design 50 (2013) 946-953. DOI: https://doi.org/10.1016/j.matdes.2013.03.066

[15] Y. Beygelzimer, V. Varyukhin, S. Synkov, D. Orlov, Useful properties of twist extrusion, Materials Science and Engineering: A 503/1-2 (2009) 14-17. DOI: https://doi.org/10.1016/j.msea.2007.12.055

[16] Y. Beygelzimer, D. Prilepo, R. Kulagin, V. Grishaev, O. Abramova, V. Varyukhin, M. Kulakov, Planar Twist Extrusion versus Twist Extrusion, Journal of Materials Processing Technology 211/3 (2011) 522-529. DOI: https://doi.org/10.1016/j.jmatprotec.2010.11.006

[17] V. Segal, Review: Modes and Processes of Severe Plastic Deformation (SPD), Materials 11/7 (2018) 1175. DOI: https://doi.org/10.3390/ma11071175

[18] K.J. Kurzydłowski, Microstructural refinement and properties of metals processed by severe plastic deformation, Bulletin of the Polish Academy of Sciences. Technical Sciences 52/4 (2004) 301-311.

[19] M.I. Latypov, E.Y. Yoon, D.J. Lee, R. Kulagin, Y. Beygelzimer, M. Seyed Salehi, H.S. Kim, Micro-structure and mechanical properties of copper processed by twist extrusion with a reduced twist-line slope, Metallurgical and Materials Transactions A 45/4 (2014) 2232-2241. DOI: https://doi.org/10.1007/s11661-013-2165-1

[20] W. H. El-Garaihy, D. M. Fouad, H. G. Salem, Multi-channel Spiral Twist Extrusion (MCSTE): A Novel Severe Plastic Deformation Technique for Grain Refinement, Metallurgical and Materials Transactions A 49/7 (2018) 2854-2864. DOI: https://doi.org/10.1007/s11661-018-4621-4

[21] S.A.A. Akbari Mousavi, A.R. Shahab, M. Mastoori, Computational study of Ti–6Al–4V flow behaviors during the twist extrusion process, Materials and Design 29/7 (2008) 1316-1329. DOI: https://doi.org/10.1016/j.matdes.2007.07.009

[22] S.A.A. Akbari Mousavi, S.R. Bahadori, A.R. Shahab, Numerical and experimental studies of the plastic strains distribution using subsequent direct extrusion after three twist extrusion passes, Materials Science and Engineering: A 527/16-17 (2010) 3967-3974. DOI: https://doi.org/10.1016/j.msea.2010.02.077

[23] J.G. Kim, M. Latypov, N. Pardis, Y.E. Beygelzimer, H.S. Kim, Finite element analysis of the plastic deformation in tandem process of simple shear extrusion and twist extrusion, Materials and Design 83 (2015) 858-865. DOI: https://doi.org/10.1016/j.matdes.2015.06.034
[24] N. Shkatulyak, Effect of twist extrusion and subsequent rolling on the texture and microstructure of aluminium alloy, International Journal of Advances in Materials Science and Engineering 3/1 (2014) 15-25.
[25] T. Bulzak, Z. Pater, J. Tomczak, K. Majerski, Technological and construction aspects of the process of hot extrusion of twist drills, Journal of Manufacturing Processes 45 (2019) 123-137. DOI: https://doi.org/10.1016/j.jmapro.2019.06.034
[26] V.V.B.Y.Y. Usov, N.M. Shkatulyak, P.A. Bryukhanov, Texture of Titanium after twist extrusion, Physics Tech. High Press. 21/3, 102-109 (in Russian).
[27] M. Nouri, H. Mohammadian Semnani, E. Emadoddin, Computational and experimental studies on the effect back pressure on twist extrusion process, Metals and Materials International 27/8 (2021) 2910-2918. DOI: https://doi.org/10.1007/s12540-020-00668-y
[28] RS Alloys Overview, 2021. Available from: https://www.rsp-technology.com/site-media/user-uploads/rsp_alloys_overview_2018lr.pdf
[29] V. Varyukhin, Y. Beygelzimer, R. Kulagin, O. Prokof'eva, A. Reshetov, Twist Extrusion: Fundamentals and Applications, Materials Science Forum 667-669 (2010) 31-37. DOI: https://doi.org/10.4028/www.scientific.net/MSF.667-669.31
[30] Y. Beygelzimer, D. Orlov, A. Korshunov, S. Synkov, V. Varyukhin, I. Vedernikova, A. Reshetov, A. Synkov, L. Polyakov, I. Korotchenkova, Features of twist extrusion: Method, structures and materials properties, Solid State Phenomena 114 (2006) 69-78. DOI: https://doi.org/10.4028/www.scientific.net/SSP.114.69
[31] S.A. Asghar, A. Mousavi, S.R. Bahador, Investigation and numerical analysis of strain distribution in the twist extrusion of pure aluminum, JOM 63/2 (2011) 69-76. DOI: https://doi.org/10.1007/s11837-011-0032-3
[32] S. Suwas, S. Mondal, Texture Evolution in Severe Plastic Deformation Processes, Materials Transactions 60/8 (2019) 1457-1471. DOI: https://doi.org/10.2320/matertrans.MF201933
[33] M. Jahedi, M.H. Paydar, S. Zheng, I.J. Beyerlein, M. Knezevic, Texture evolution and enhanced grain refinement under high-pressure-double-torsion, Materials Science and Engineering: A 611 (2014) 29-36. DOI: https://doi.org/10.1016/j.msea.2014.05.081
[34] A.P. Zhilyaev, T.R. McNelley, T.G. Langdon, Evolution of microstructure and microtexture in fcc metals during high-pressure torsion, Journal of Materials Science 42/5 (2007) 1517-1528. DOI: https://doi.org/10.1007/s10853-006-0628-0
[35] A. Macháčková, Decade of Twist Channel Angular Pressing, A Review, Materials 13 (2020) 1725. DOI: https://doi.org/10.3390/ma13071725
[36] R. Kocich, Deformation behavior of Al/Cu Cl and composite during twist channel angular pressing, Materials 13/18 (2020) 4047. DOI: https://doi.org/10.3390/ma13184047
[37] S. Sanamar, H.-G. Brokmeier, N. Schell, Texture Gradient in a Rectangular Extruded Al60Mg40 Metal Matrix Composite, Metals 9/2 (2019) 167. DOI: https://doi.org/10.3390/met9020167
[38] W. Zhang, H. Zhang, L. Wang, J. Fan, X. Li, L. Zhu, S. Chen, H.J. Roven, S. Zhang, Microstructure Evolution and Mechanical Properties of AZ31 Magnesium Alloy Sheets Prepared by Low-Speed Extrusion with Different Temperature, Crystals 10/8 (2020) 644. DOI: https://doi.org/10.3390/cryst10080644
[39] O. Hilšer, S. Rusz, P. Szkandera, L. Čížek, M. Kraus, J. Džugan, W. Maziarz, Study of the Microstructure, Tensile Properties and Hardness of AZ61 Magnesium Alloy Subjected to Severe Plastic Deformation, Metals 8/10 (2018) 776. DOI: https://doi.org/10.3390/met8100776
[40] Y. Wu, B. Deng, T. Ye, W. Liu, Z. Nie, X. Zhang, Effect of Pass Strain on the Microstructure, Texture and Mechanical Properties of AZ31 Magnesium Alloy Fabricated by High Strain Rate Multiple Forging, Metals 10/8 (2020) 1000. DOI: https://doi.org/10.3390/met10081000
[41] T. Aizawa, T. Yoshino, T. Inohara, Micro-/Nano-Texturing of Aluminum by Precise Coining for Functional Surface Decoration, Metals 10/8 (2020) 1044. DOI: https://doi.org/10.3390/met10081044
[42] C. Yang, Y. Mei, D. Meng, G. Zhu, S. Liu, Y. Peng, L. Wu, C. Zha, B. Shi, Mechanical Anisotropy Induced by Strain Path Change for AZ31 Mg Alloy Sheet, Metals 10/8 (2020) 1049. DOI: https://doi.org/10.3390/met10081049